

## Stitched $m \times 96$ $7\mu\text{m}$ pixel TDI sensor

Lei Wu<sup>1</sup>, Nixon O<sup>1</sup>, Cees Draijer<sup>2</sup>, Jan Bosiers<sup>2</sup>, Harry van Kuijk<sup>2</sup>, Holger Stoldt<sup>2</sup>

DALSA Corporation

<sup>1</sup> 605 McMurray Road, Waterloo, ON, N2V 2E9, Canada

Tel.: (519) 886-6000, Fax: (519) 886-5767, E-mail: [lei.wu@dalsa.com](mailto:lei.wu@dalsa.com)

<sup>2</sup> High Tech Campus 12a, M/S 01, 5656 AE Eindhoven, The Netherlands

Tel.: +31 40 274 5600, Fax: +31 40 274 4090

### Abstract

A family of TDI sensors based on stitched design blocks is presented. Devices of varying sizes and configurations are built from a common design block in a single mask set. The design block has  $7\mu\text{m}$  pixels, 96 TDI stages (fewer stages can be selected), 100x vertical antiblooming, >80,000 electron full well, operates at a data rate of 40 MHz per output achieving a scan rate of 73 kHz, and has a responsivity of  $520\text{ V}/(\mu\text{J}/\text{cm}^2)$  at 520nm. The sensor combines high resolution with very high speed and high responsivity, all essential requirements for many demanding machine vision applications.

### 1. Sensor Architecture

The block diagram of an 8,192 pixel, 16 output sensor (one of the many possible variants in this stitched family) is shown in Fig. 1.

The die is fabricated by stitching design blocks using the approach described in [1]. Each design block consists of 2,048 TDI columns that can be stitched to create TDI sensors with length limited only by the size of the wafer. As in stitched area arrays, the stitch boundary has to be designed carefully so that the seam does not produce undesirable image artifacts.

The  $7\mu\text{m}$  pixel pitch is important because this makes high resolution (8K and 12K columns) TDI array systems economically feasible. Earlier generations of DALSA TDI arrays have 10 or 13  $\mu\text{m}$  pixels. Other commercially available TDI arrays have  $>8.5\mu\text{m}$  pixels. If the pixel pitch were much larger than  $7\mu\text{m}$ , the imager will be too long for the size of the lens to be economically practical.

In order to squeeze the readout circuitry along the length of the array, portions of the horizontal CCD are designed to be less than  $7\mu\text{m}$  wide.

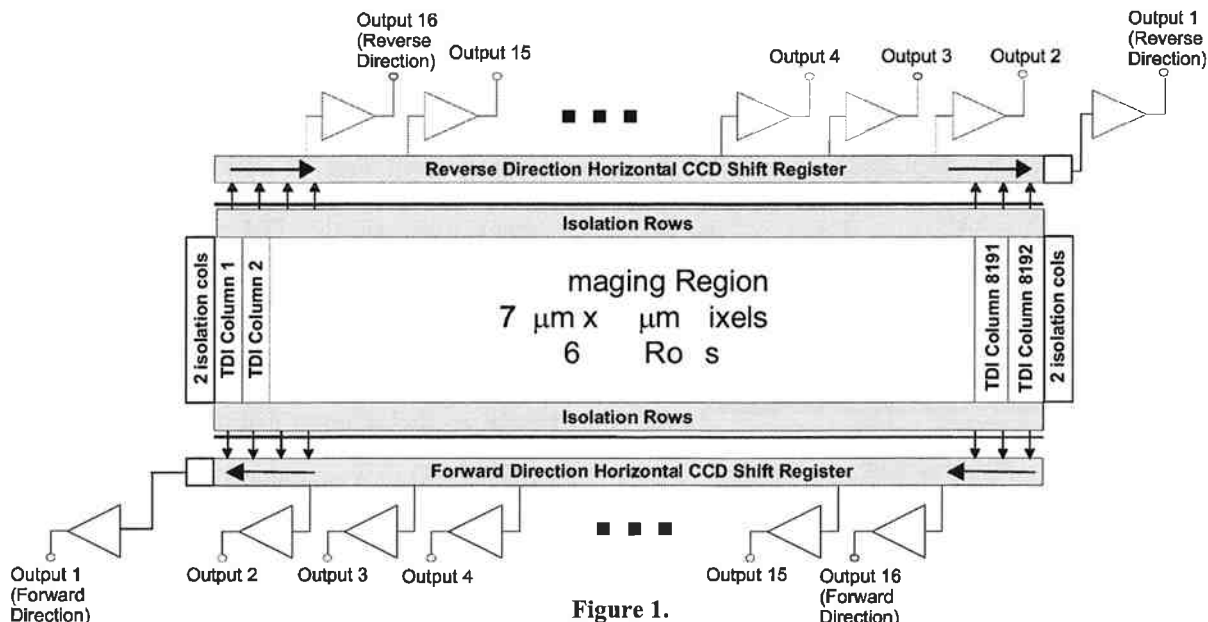


Figure 1.  
Sensor Block Diagram.

We have designed two variants: the first with one active output every 1,024 TDI columns and the second with one active output every 512 TDI columns. We indicate “active” output because the design allows bi-directional TDI scanning and hence requires outputs on both sides of the array. Only one output per side is active at any given time.

The blocks are designed to be independently clocked and biased. The speed performance of the devices is independent of the number of stitching blocks used. The devices operate with a 40 MHz data rate. This, along with a 2.2 MHz vertical clock frequency, allows sensor variants with one active output every 512 TDI columns to achieve a scan rate of 73 kHz.

The device architecture allows the selection of 16, 32, 48, 64, 80, or 96 TDI stages through the use of the vertical antiblooming drain [2]. If fewer than 96 stages are selected, unwanted charges are drained at appropriate row locations through the vertical antiblooming drain to the substrate.

## 2. Sensor Performance

A summary of measured performance is shown in Table 1.

The devices are fabricated using a process similar to the membrane poly process described in [3] and possess the enhanced response and low dark current advantages of this process. The spectral response is shown in Fig. 2.

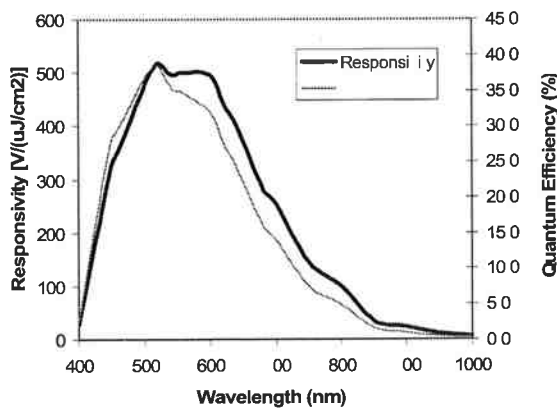


Figure 2.  
Spectral Response.

With a charge conversion efficiency of  $11\mu\text{V}/e$  at the sensor output, the sensor achieves a peak responsivity of  $520\text{V}/(\mu\text{J}/\text{cm}^2)$  and a peak quantum efficiency of 38% at 520 nm.

Narrow tungsten metal buses are used to provide a low resistance path to the polysilicon gates. These buses run vertically along the channel stops, resulting in a fill factor of  $\sim 90\%$ .

The  $\sim 90\%$  horizontal fill factor results in a  $\sim 10\%$  difference between the horizontal and vertical MTF at Nyquist, as shown in Fig. 3. The vertical MTF is measured with the sensor operated as an area array.

The narrow metal bus is perhaps the source of the difference in the structures of the horizontal and vertical MTF curves. The vertical metal bus is approximately 700 nm wide. This dimension is almost the same as the 660 nm wavelength of illumination used during the MTF measurement. The diffraction patterns resulting from the narrow metal line may explain the deviation from the ideal MTF [4].

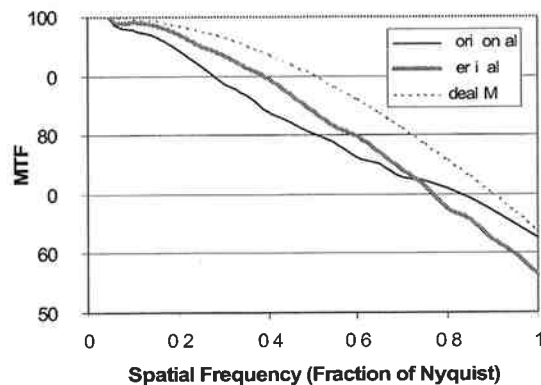
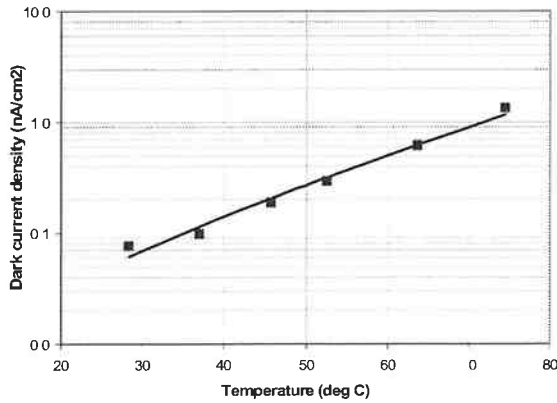


Figure 3.  
MTF at 660 nm.

In TDI arrays, particularly in ones that have a high electron-to-voltage charge conversion factor, it is important that the dark current density be low. This is because the TDI output sums the dark current from all the TDI stages, making the effective dark current collection area large.

Unlike area imagers, TDI photogates cannot be pinned to reduce the dark current [5]. This is because the stage selection gates need to be pinned so that charges that attempt to cross the stage selection gates will be drained to the substrate. DALSA produces other TDI arrays that can operate in the MPP mode. These have low dark current levels also. However, stage selection is not possible with these devices since all gates are pinned during integration. In this new TDI family, to minimize dark current and still allow stage selection, we have to ensure that the dark

current is low even when the surface is not pinned.



**Figure 4.**  
**Dark Current Density.**

The sensor is designed with a sufficient density of hydrogen entry points to allow uniform passivation of surface states [3]. The dark current density is shown in Fig. 4. The dark current is uniform and does not contribute significantly to FPN.

Continuous improvements in our wafer fabrication processes have resulted in this TDI array family having much lower non-uniformity than earlier generations of TDI arrays, despite having a larger number of pixels and a smaller pixel pitch. The maximum PRNU specification for this sensor is 5% of the output peak-to-peak. This number includes all pixels. The output

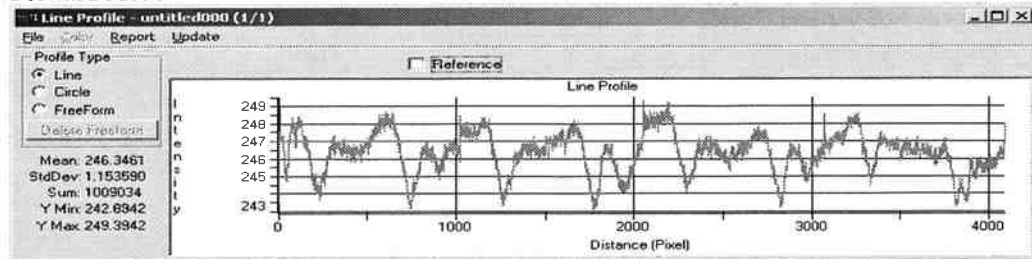
response profile from a 4,096 pixel sensor is shown in Figure 5. In this figure, the scale has been expanded to make the non-uniformity more visible. Because the array can operate in two scanning directions, we have shown the non-uniformity in both scanning directions. Note that the sensor does not exhibit a bow-shaped non-uniformity that affects many imaging arrays.

The sensor has 900 mV or  $\sim 82,000$  electrons of guaranteed linear unsaturated response. When biases are optimized for each batch, it is possible to achieve up to 1,200 mV of unsaturated output.

Despite having a small pixel pitch, the horizontal CCD utilizes 2-phase shift registers to minimize the number of clock feedthroughs in the analog output waveform. Minimizing clock feedthroughs improves sampling stability and minimizes the noise in the sampled output. This, along with other design choices to minimize noise, allows the camera using this sensor to achieve a dynamic range of 64 dB at an output data rate of 40 MHz.

A small section of an image acquired using this sensor is shown in Fig. 6. The bars labelled "7.1" are at around 50% of Nyquist. These patterns are still quite sharp at this spatial frequency.

**Forward Mode**



**Reverse Mode**

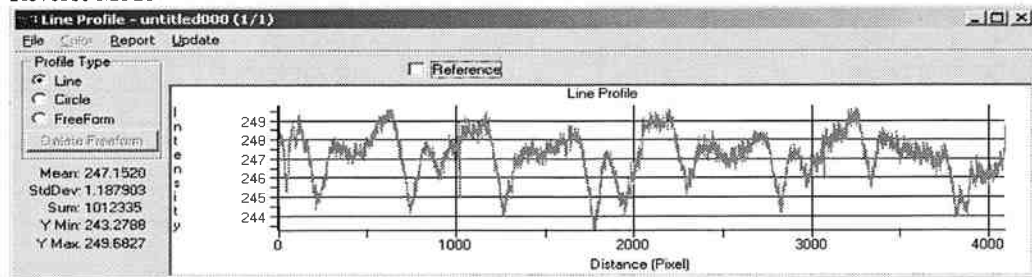


**Figure 5.**  
**Sensor Non-Uniformity Profile.**

The distance (pixel) numbers in the forward and reverse plots represent the same physical columns.

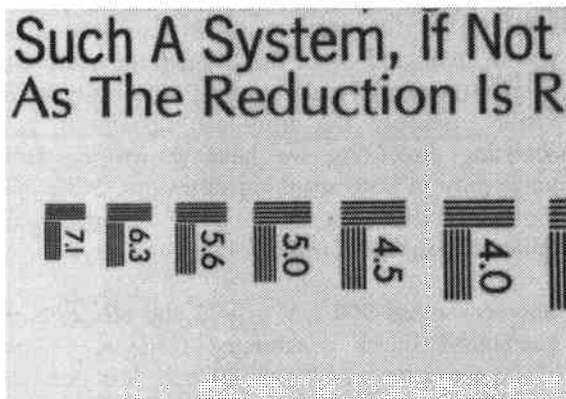


Figure 6.  
Section of Image Captured Using this Sensor.

### 3. Conclusions

We present a stitched family of TDI arrays. The  $7\ \mu\text{m}$  pixel size permits resolution of up to 12k pixels. The array has low dark current, operates at high data rates, has low noise, has antiblooming, and has a selectable number of TDI stages.

### 4. References

- [1] G. Kreider and J. Bosiers, "An  $mK \times nK$  bouwblok CCD image sensor family. I. Design", IEEE Trans. on Electron Devices, vol. 49, no. 3, March 2002, pp. 361-369.
- [2] G. Weale, M. Kiik, E. Fox, C. Flood, and S. Ingram, "Anti-blooming optimization using simulations and measurements for a VAB process", 1997 IEEE Workshop on Charge-Coupled Devices and Advanced Image Sensors, 1997, P-14.
- [3] H. Peek, D. Verbugt, and H. Heijns, "A Low Dark Current Double Membrane Poly-Si FT-Technology for 2/3 Inch 6M Pixel CCD Imagers", IEDM 1999, pp. 871-874.
- [4] M. Ledgerwood, internal DALSA communication.
- [5] J.T. Bosiers, E. Roks, H.L. Peek, A.C. Kleimann and A.G. van der Sijde, "An S-VHS Compatible 1/3" Color FT-CCD Imager with Low Dark Current by Surface Pinning", IEEE Transactions on Electron Devices, vol. 42, no. 8, Aug. 1995, pp. 1449-1460.

Parameter	Value
Pixel size	$7\ \mu\text{m} \times 7\ \mu\text{m}$
Number of TDI stages	Selectable: 16, 32, 48, 64, 80, or 96
TDI scan direction	Bi-directional
Pixel output rate	$40\ \text{MHz} \times (\text{No. of TDI columns} / 512)$
Frequency of horizontal clocks	40 MHz
Horizontal clock swing	5V
Frequency of vertical clocks	2.2 MHz
Vertical clock swing	12V
TDI scan rate	Up to 73 kHz
Horizontal CTE	$> 0.99999$
Vertical CTE	$> 0.99998$
Charge conversion efficiency	$11\ \mu\text{V}/e$
Peak responsivity at 520 nm	$520\ \text{V}/(\mu\text{J}/\text{cm}^2)$
Quantum efficiency at 520 nm	38%
Fill well capacity	$> 80,000$ electrons
Saturation voltage	$> 900\ \text{mV}$
Dynamic range	67 dB
Fixed pattern noise	$< 100$ electrons at $65^\circ\text{C}$
Photoresponse non-uniformity	$< 5\%$ of signal peak-to-peak, includes seam artifacts
Antiblooming	100x

Table 1.  
Device Parameters and Measured Performance Characteristics.